# Reflecting metagrating-enhanced thin-film organic light emitting devices

Cite as: Appl. Phys. Lett. **118**, 053302 (2021); https://doi.org/10.1063/5.0034573 Submitted: 21 October 2020 . Accepted: 13 January 2021 . Published Online: 01 February 2021

Daniel Wasserman, Andrea Alù, and Ananth Dodabalapur







### **ARTICLES YOU MAY BE INTERESTED IN**

Will flat optics appear in everyday life anytime soon?
Applied Physics Letters 118, 100503 (2021); https://doi.org/10.1063/5.0039885

Optically tunable all-silicon chiral metasurface in terahertz band Applied Physics Letters 118, 051101 (2021); https://doi.org/10.1063/5.0039992

Expanding the understanding of organic electrochemical transistor function Applied Physics Letters 118, 053301 (2021); https://doi.org/10.1063/5.0039345

☐ QBLOX



Shorten Setup Time
Auto-Calibration
More Qubits

Fully-integrated
Quantum Control Stacks
Ultrastable DC to 18.5 GHz
Synchronized <<1 ns
Ultralow noise



100s qubits

visit our website >



## Reflecting metagrating-enhanced thin-film organic light emitting devices

Cite as: Appl. Phys. Lett. **118**, 053302 (2021); doi: 10.1063/5.0034573 Submitted: 21 October 2020 · Accepted: 13 January 2021 · Published Online: 1 February 2021







Xin Xu, <sup>1</sup> (i) Hoyeong Kwon, <sup>1</sup> (ii) Stanley Finch, <sup>1</sup> Jae Young Lee, <sup>1,a)</sup> Leland Nordin, <sup>1</sup> (ii) Daniel Wasserman, <sup>1</sup> (ii) Andrea Alù, <sup>1,2</sup> (ii) and Ananth Dodabalapur<sup>1,b)</sup> (ii)

#### **AFFILIATIONS**

- Department of Electrical and Computer Engineering, The University of Texas at Austin, Austin, Texas 78712, USA
- <sup>2</sup>Photonics Initiative, Advanced Science Research Center, City University of New York, New York, New York 10031, USA
- <sup>a)</sup>Permanent Address: Samsung Display Co., Ltd., Gyeonggi-do 17113, South Korea.
- <sup>b)</sup>Author to whom correspondence should be addressed: ananth.dodabalapur@engr.utexas.edu

#### **ABSTRACT**

Organic light emitting diodes can achieve close to unitary internal quantum efficiency; however, their external quantum efficiency is much lower due to losses within the device. Gradient metasurfaces and metagratings can be utilized to achieve substantial electromagnetic field manipulation and enhancement of the local density of photonic states, thereby improving the external quantum efficiency of organic light emitting devices. In this work, we show how suitably designed reflecting plasmonic metagratings can be potentially incorporated into a top-emitting organic light emitting device, resulting in large enhancement of light emissivity by effectively coupling out the light trapped in the waveguide modes. We describe how both periodic and quasiperiodic metagratings can be used to improve device performance. Electromagnetic simulations and measurements show that our metagratings greatly enhance the electromagnetic field intensity in the light emission layer, leading to increased emission normal to the plane of the layers (by up to a factor of 4.8) and suppression of light trapping typically lost into waveguide modes.

Published under license by AIP Publishing. https://doi.org/10.1063/5.0034573

One of the major factors that limit the external quantum efficiency in organic LEDs (OLEDs) is the light lost due to waveguide and surface plasmon modes. Many solutions have been proposed to enhance the efficiency of outcoupling emission in bottom-emitting OLEDs (which emit through the glass substrate), for example, using planar microcavities, lens sheets, photonic crystals, indexengineered substrates, etc. For top-emitting LEDs, increasing the efficiency of outcoupling is far more difficult since we cannot easily integrate additional structures on top of the device. In this work, we show that a reflecting metagrating, consisting of a combination of metallic and dielectric materials, placed underneath the active layers provides an effective way to increase the outcoupling efficiency for top-emitting organic thin films and provides a framework for increasing top-emitting OLED efficiency in the future.

Metagratings are periodic arrays of nanostructured inclusions tailored to enhance the way in which light interacts with ultrathin structured surfaces by relying on the combination of exotic light–matter interactions at the unit cell level and grating resonances at the lattice level.<sup>8–12</sup> They have been shown to overcome inherent efficiency limits in light manipulation of more conventional gradient metasurface

approaches, <sup>13,14</sup> with the additional advantage of relying on unit cell sizes comparable with the operating wavelength, which enhances the bandwidth and provides more resilience to material loss. In this study, we utilize metal/dielectric metagratings to enhance the outcoupling efficiency of top-emitting organic devices. By designing the metagrating to work as a shunt admittance in the organic emission layer, we can effectively couple out the light trapped in the waveguide mode toward the normal propagation direction. We first consider metagratings with a periodic square lattice, and we then explore quasiperiodic designs to achieve large light emissivity with near zero-net polarization.

Figure 1(a) shows the metagrating structure under analysis, consisting of a two-dimensional grating backed by a conducting plane and a spacer. In this work, we consider both quasiperiodic and periodic 2D patterns containing metals and dielectric materials. The overall geometry of the considered layered structure is shown in Fig. 1(b), which illustrates the integration of the metagrating within the proof-of-concept top emitting organic device. A top-emitting OLED is shown in Fig. 1(c) as a helpful comparison with the proof-of-concept device. The device structure of Fig. 1(b), used in all the experiments described in this Letter, paves the way for integrating a metagrating into a

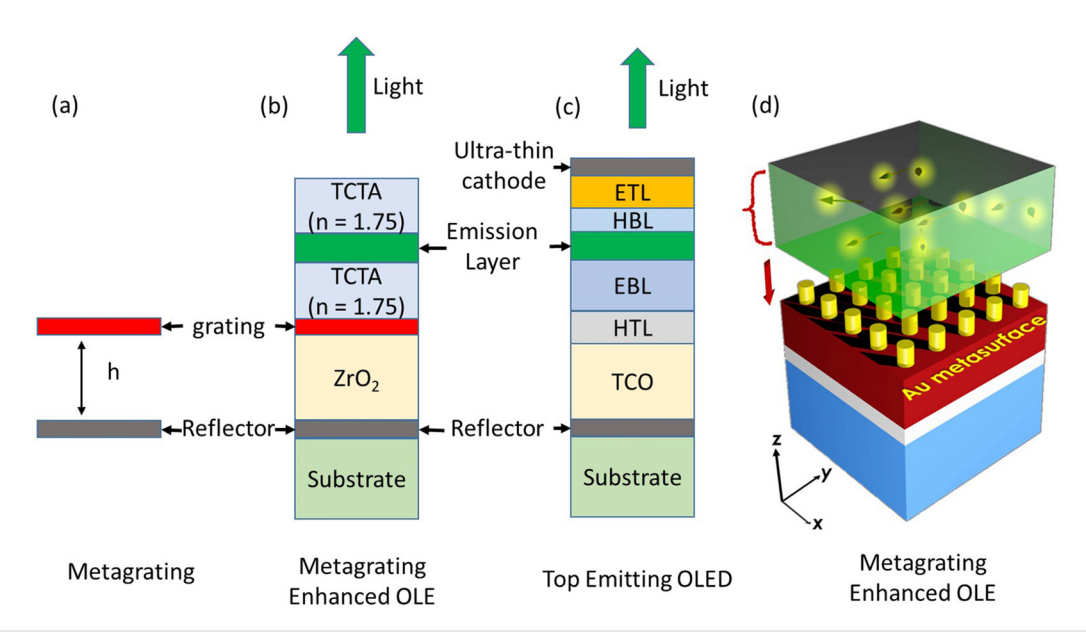


FIG. 1. (a) Schematic layer structure of a 2D metagrating placed above a metal reflector (ideally a perfect electrical conductor) and separated from it by a distance h; (b) the layer structure of the metagrating light emitting devices used in this study. The bottom metal reflector is a silver mirror deposited by evaporation. The ZrO<sub>2</sub> layer is the optical analogue of transparent conducting oxides such as ITO typically used as anodes on OLEDs. The TCTA layers are transparent organics that mimic equivalent layers in an OLED device. The emission layer is composed of 50 nm of 8-hydroxyquinolinato aluminum (Alq). (c) Layer structure of a top emitting OLED taken from the literature with a back reflector added. The HTL (hole transporting layer), EBL (electron blocking layer), HBL (hole blocking layer), and ETL (electron transport layer) are all thin organic layers. The emission layer often consists of a semiconductor such as Alq with a dopant. (d) 3D sketch of the metagrating integrated organic light emitting device.

realistic electroluminescent device and is helpful for demonstrating the benefits of its exotic wavefront manipulation. Figure 1(d) shows a 3D schematic of our device structure.

The considered metagrating patterns consist of a two-dimensional square grating of gold cylinders, shown in Fig. 2(a), and a quasicrystal pattern with fivefold symmetry, shown in Fig. 2(b). This second metagrating enables polarization-independent enhancement, as detailed in the following. The space between the gold cylinders and the reflecting backplane was filled with ZrO2, a solution-deposited dielectric. In all our structures, light is emitted from a 50-nm thick layer of 8hydroxyquinolinato aluminum (Alq), a broad-band organic emitter.<sup>15</sup> Photoexcited luminescence was measured using a microscope/camera and a fiber-coupled spectrometer. The optical excitation is provided by a 405 nm laser, as shown in Fig. 2(c). Surface normal emission was imaged using a camera through a monoscope with adjustable magnification. This arrangement allows accurate comparison of intensities relative to conventional devices without metasurface loading and the use of statistical averaging of a large number of individual measurements to greatly improve accuracy. The use of a series of bandpass filters placed between the devices and the microscope allows transforming the broadband emission into a series of relatively narrow-band emitted beams with a linewidth of 10 nm in the range of 470 nm-630 nm, in order to analyze the wavelength dependence of the light emission. We also used polarization filters to study the degree of polarization of emitted light. The angular dependence of intensity and spectral line shapes was analyzed using a different setup, described in the supplementary material.

Surface-normal emission intensity enhancement for a 320 nm period square lattice metagrating device is shown in Fig. 3(a) for different spacer thicknesses. A physical length of 320 nm corresponds to an

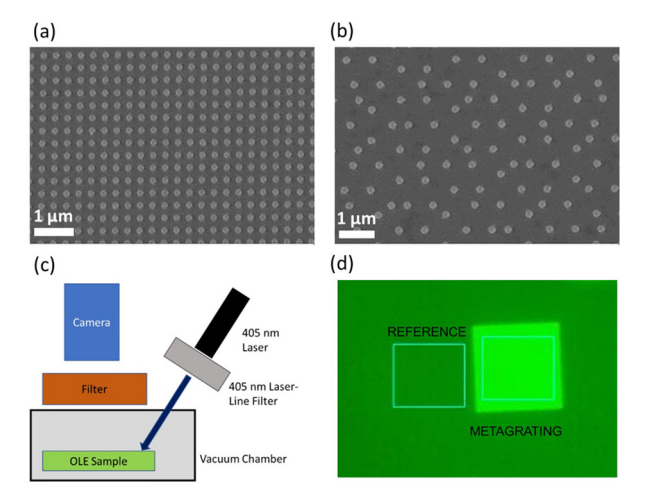
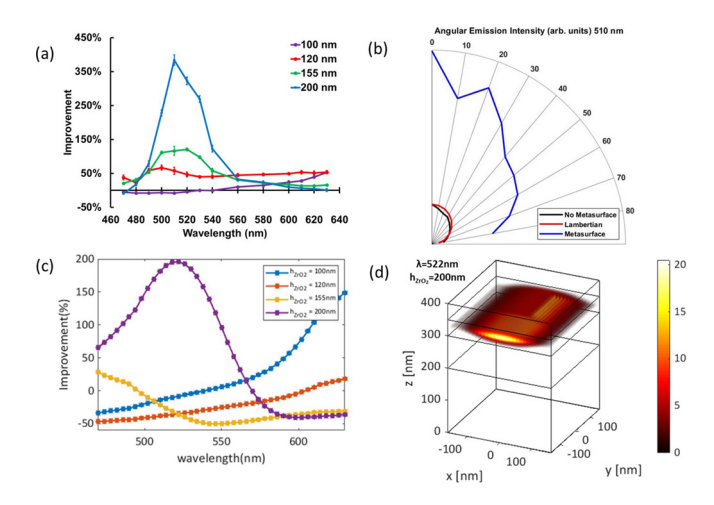


FIG. 2. (a) Square lattice metagrating consisting of Au cylinders of diameter 180 nm and height 50 nm with a center-to-center spacing of 320 nm; (b) 2D quasiperiodic metasurface of Au cylinders. The details of the geometry of the quasicrystal are described in the supplementary material; (c) experimental setup to measure surface-normal emission. Light from a 405 nm laser is incident on the sample, resulting in emission for the Alq layer (the only material that emits light in the visible). The samples are kept in a vacuum chamber to suppress degradation. A camera images light emitted by the samples through a microscope. (d) Typical images contain emission from both metasurface areas and adjacent nonmetasurface areas facilitating quantitative comparison. In this case, the bright emission is from a square metasurface with a periodicity of 320 nm taken with a bandpass filter centered at 520 nm (10 nm FWHM). The surrounding light of lower intensity is from the nonmetasurface areas but containing the back reflector. We typically average 100 images to get a very accurate comparison. The individual images differ in terms of small adjustments to the laser position and angle.



**FIG. 3.** (a) Enhancement in intensity of the metasurface devices with a square 320 nm period lattice relative to a nonmetasurface device located on the same substrate and very close. Each data point represents the average of 100 measurements. The data are shown for different thicknesses of ZrO<sub>2</sub>, which also represents the distance between the back reflector and the grating; (b) angular dependence of the intensities in the metasurface sample and a nonmetasurface sample that is otherwise identical. The description of the angular dependence measurement setup is given in the supplementary material. The intensities at normal emission are measured as described in Fig. 2(c) and used as the basis for comparison between the two samples; (c) simulated results of expected improvement in surface-normal light emission intensity at varying thicknesses of ZrO<sub>2</sub>. (d) The simulated electromagnetic field enhancement distribution at the wavelength with the highest intensity enhancement for a 200 nm spacer.

optical length that is matched to the peak emission wavelength of Alq. A 0% enhancement means that the intensities of the nonmetasurface and metasurface areas (both of which have the same silver backreflector) are the same, while a 100% enhancement means that the metasurface device has twice the intensity. The maximum measured intensity enhancement is 380% (or 4.8×) for a spacer thickness of 200 nm at 510 nm. The function of the spacer is to control the number of leaky and guided modes that the emitted light can couple into. A thicker spacer implies a larger number of modes and a larger peak enhancement up to an optimal value. The angular dependence, shown in Fig. 3(b), provides further evidence for the enhancement mechanism: the normal emission intensity is enhanced, while the off-axis intensity drop-off is not too steep after an initial sharp decline. The enhanced intensity in the normal direction is compensated by reduced propagation along the in-plane direction.

The presence of the metagrating modifies the electromagnetic field distribution within the thin film emitting device in a nontrivial manner. Its tailored response suppresses the coupling of electromagnetic power into waveguide modes and instead redirects the energy to maximize emission out of the device. We used COMSOL Multiphysics to model the electromagnetic fields within the thin film device. It is computationally difficult to model randomly oriented dipoles to accurately model the emission in an organic material, and so we used two simplified models to demonstrate the underlying electromagnetic phenomena. In the first model, we leveraged the principal of reciprocity and performed numerical calculations for plane wave excitation in Fig. 2(a). Based on reciprocity, we can estimate the emission

enhancement toward the normal direction for a given polarization by evaluating the average field enhancement induced in the organic emission layer due to plane wave excitation from normal incidence with the polarization of interest. The results for field enhancement as a function of wavelength and spacer thickness are shown in Fig. 3(c), while Fig. 3(d) shows the field distribution at the peak enhancement for a 200 nm spacer. Here, we plot the field intensity ratio in the organic emission layer, normalized to the case without the metagrating. Figure 3(c) shows that the metagrating is most efficient around the wavelength of 522 nm with a spacer thickness of 200 nm, which is close to the optimal response achieved experimentally, with a peak enhancement at 510 nm. The slight difference is due to the uncertainty in the geometrical parameter estimation, such as layer thicknesses and refractive indices. We note that the spontaneous emission peak of Alq without metagrating is near 540 nm. The enhancement is rather broadband, in accordance with the metagrating properties.<sup>16</sup> The 3D field profile in Fig. 3(d) shows the field enhancement efficiency at each point of the organic emission layer, which shows how the metasurface helps confine the field inside the organic emission layer, offering up to a 20-fold field enhancement. The enhanced field in the organic layer is a result of the redirection of electromagnetic power from lateral waveguide modes toward radiation modes.

To show more explicitly that the enhancement of the electromagnetic field is due to the metagrating coupling out electromagnetic energy from lateral waveguide modes into emission modes, we also studied the emission of five small dipoles polarized in the x–y plane within the organic emission layer and calculated the field intensity in the far-field, as shown in Fig. 4(a). As expected in this scenario, the emission enhancement peaks in the same wavelength range, with an enhancement factor around 10 in terms of radiated power, shown in Fig. 4(b).

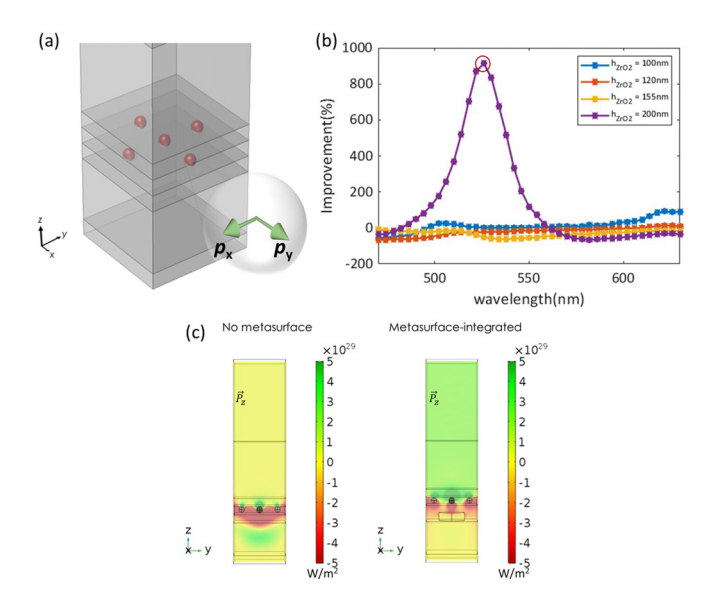


**FIG. 4.** (a) Simulation arrangement of five dipole emitters. The dipole emitters all emit in phase and are polarized to x- and y-axes. (b) Surface normal power emission improvement from simulation with dipole emitters in (a). (c) Poynting vector normal to the xy plane evaluated at the point circled in (b). The left figure shows the result without metagrating, and the right figure shows the metagrating integrated result

Figure 4(c) compares the power flow distribution in the near-field of the emitting layer with and without metagrating, confirming significant enhancement in emission and reduced trapping into waveguide modes within the device. These calculations show that laterally propagating waveguide modes are dramatically suppressed in the metasurface device structure, leading to higher efficiencies.

The response of these periodic devices exhibits a polarization dependence, which may not be suitable for some applications. To retain the advantages of a metasurface architecture, but with less polarization selectivity, we experimented using quasicrystal metagratings. Figure 5(a) shows the response of a 2D quasicrystal metagrating, with detailed dimensions described in the supplementary material. The degree of intensity enhancement in the quasicrystal is lower than that in the corresponding periodic structure, but it occurs over a broader range of wavelengths. Importantly, the angular dependence of emission intensity falls off more slowly. Figure 5(b) shows the emission intensity in the normal direction for a quasicrystal metagrating organic emission device and the same device without metagrating. The degree of polarization is shown in Fig. 5(c) as a function of wavelength, showing again a lower enhancement compared to a periodic metagrating, shown in Fig. 5(d), but over a broader bandwidth.

Key to our approach is that our patterning and integration of 2D metasurfaces into light emitting devices is done before the sensitive organic layers are deposited. We use  $ZrO_2$  (n = 1.7–2.0) to mimic the optical properties of transparent conducting oxides, such as indium tin oxide, which are commonly used as anodes in OLEDs. Tris(4-

carbazoyl-9-ylphenyl)amine (TCTA), one of the materials we employ in our structures, is a commonly used charge transport layer in OLEDs. <sup>17</sup> The overall thickness of the organic layers is similar to that in a top emitting OLED. <sup>7</sup> It is possible to incorporate such metasurfaces in OLEDs since the metasurface patterning occurs before the organic layers are deposited. We note that only one step of high-resolution patterning is necessary to define the metal geometry, which we have achieved using electron beam lithography. For future large-scale implementations, similar results can be achieved using scalable high-throughput nanomanufacturing techniques such as deep-UV photolithography for OLEDs on silicon substrates and nanoimprint lithography<sup>18</sup> for glass and plastic substrates. The feature sizes used in the metagratings can be conveniently realized by both types of lithography.

We can go beyond efficiency enhancement and also tailor the directionality of the emitted light to suit a particular application. For example, when a high intensity of surface normal emission is desired as in augmented reality displays, periodic metasurfaces will be helpful, whereas for conventional displays, in which polarized light emission is not desirable, quasicrystal metasurfaces will work very well and also provide a significant efficiency boost. High surface normal emission intensities will also be useful in down-converting display elements in which blue light is generated and down-converted to green or red light by phosphors such as core–shell nanocrystals. <sup>19</sup>

We have found that the reflectivity of silver, the distance between the silver reflector and the metagrating, and the metagrating geometry (lateral dimensions and vertical height) are all important parameters

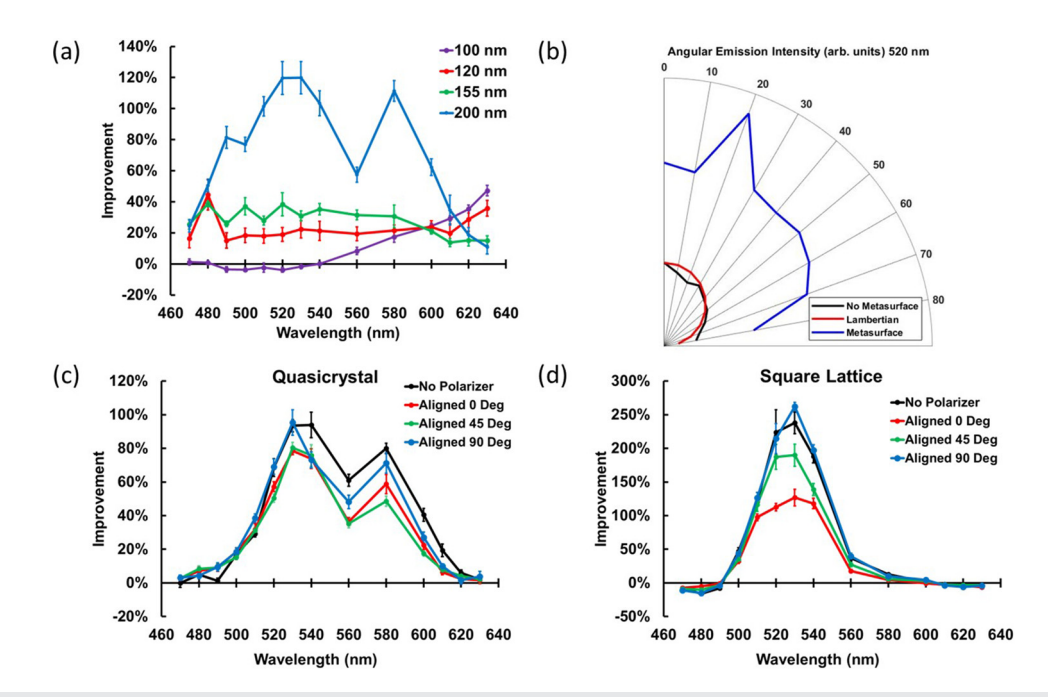


**FIG. 5.** (a) Enhancement in intensity of the metasurface devices with a quasiperiodic lattice relative to a nonmetasurface device located on the same substrate and very close. Each data point represents the average of 100 measurements. The data are shown for different thicknesses of  $ZrO_2$ , which also represent the distance between the back reflector and the metasurface; (b) angular dependence of the intensities in the quasicrystal metasurface sample and a nonmetasurface sample that is, otherwise, identical. The intensities at normal emission are measured as described in Fig. 2(c) and used as the basis for comparison between the two samples; (c) polarization in the emitted light from a quasicrystal metasurface device relative to a nonmetasurface device. Data are shown for the case of no polarizer and for linear polarizers aligned along different directions. The polarizers are placed between the sample and the microscope. (d) Polarization in the emitted light from the square lattice metagrating.

in determining the overall performance characteristics, including directionality, efficiency enhancement, and bandwidth. Increasing both the silver reflectivity and the distance between the back reflector and the metasurface results in increased intensity enhancement in the normal direction. Additional variables that can have impact include changing the metagrating composition and exploring other periodic patterns such as triangular or hexagonal lattices and honeycomb lattices. We have used a quasicrystal design with fivefold symmetry. Other designs are also possible with higher folds of symmetry, potentially resulting in even less polarized emission.

In this Letter, we have focused on a structure light emitting device involving organic semiconductors similar to those in OLEDs to demonstrate the potential of the metagrating approach. This is an important first step toward integration into a full topemitting OLED. It is also possible to have alternative emission materials, such as core–shell nanoparticles, <sup>19</sup> or other inorganic or perovskite light emitting materials. <sup>20</sup> While the device geometry employed here is modeling a top-emitting OLED, we can also integrate metasurfaces in other kinds of light-emitting devices such as light emitting transistors<sup>21</sup> and future hybrid nanomodular devices using 2D materials. Reflecting metasurfaces are easy to incorporate because they are fabricated before the sensitive organic layers and result in major improvements for relevant figures of merit of light emitting devices.

See the supplementary material for details about the angulardependent emission measurement setup and details about the quasicrystal pattern generation used to create the quasicrystal metagratings.

X.X. and A.D. acknowledge financial support from Samsung Display Co., Ltd. We also acknowledge financial support from the National Science Foundation, NSF Grant No. CMMI1938179. D.W. and L.N. gratefully acknowledge support from the National Science Foundation (ECCS-1926187). The work was partly done at the Texas Nanofabrication Facility supported by NSF Grant NNCI-1542159.

#### **DATA AVAILABILITY**

The data that support the findings of this study are available from the corresponding author upon reasonable request.

#### **REFERENCES**

- <sup>1</sup>H. Kaji, H. Suzuki, T. Fukushima, K. Shizu, K. Suzuki, S. Kubo, T. Komino, H. Oiwa, F. Suzuki, A. Wakamiya, Y. Murata, and C. Adachi, Nat. Commun. 6, 8476 (2015).
- <sup>2</sup>R. Meerheim, M. Furno, S. Hofmann, B. Lüssem, and K. Leo, Appl. Phys. Lett. **97**, 253305 (2010).
- <sup>3</sup>A. Dodabalapur, L. J. Rothberg, R. H. Jordan, T. M. Miller, R. E. Slusher, and J. M. Phillips, J. Appl. Phys. 80, 6954 (1996).
- <sup>4</sup>J. H. Han, J. Moon, D. H. Cho, J. W. Shin, H. Y. Chu, J. I. Lee, N. S. Cho, and J. Lee, J. Inf. Disp. **19**, 179 (2018).
- <sup>5</sup>Y. S. Shim, J. H. Hwang, C. H. Park, S.-G. Jung, Y. W. Park, and B.-K. Ju, Nanoscale **8**, 4113 (2016).
- <sup>6</sup>S. Reineke, F. Lindner, G. Schwartz, N. Seidler, K. Walzer, B. Lüssem, and K. Leo, Nature 459, 234 (2009).
- 7S. Hofmann, M. Thomschke, B. Lüssem, and K. Leo, Opt. Express 19, A1250 (2011).
- <sup>8</sup>V. Neder, Y. Ra'Di, A. Alù, and A. Polman, ACS Photonics 6, 1010 (2019).
- <sup>9</sup>Y. Ra'di, D. L. Sounas, and A. Alù, Phys. Rev. Lett. **119**, 067404 (2017).
- 10 Y. Ra'di and A. Alù, ACS Photonics 5, 1779 (2018).
- <sup>11</sup>D. Sell, J. Yang, S. Doshay, R. Yang, and J. A. Fan, Nano Lett. 17, 3752 (2017).
- <sup>12</sup>J. Yang, D. Sell, and J. A. Fan, Ann. Phys. **530**, 1700302 (2018).
- <sup>13</sup>X. Xu, H. Kwon, B. Gawlik, N. Mohammadi Estakhri, A. Alù, S. V. Sreenivasan, and A. Dodabalapur, Nano Lett. 18, 3362 (2018).
- <sup>14</sup>N. Mohammadi Estakhri and A. Alù, Phys. Rev. X **6**, 041008 (2016).
- <sup>15</sup>P. Dalasinski, Z. Lukasiak, M. Rebarz, M. Wojdyla, A. Bratkowski, and W. Bala, Opto-Electron. Rev. 12, 429 (2004).
- <sup>16</sup>H. Kwon, H. Chalabi, and A. Alù, Nanomater. Nanotechnol. 9, 1 (2019).
- <sup>17</sup>J. Ràfols-Ribé, P. A. Will, C. Hänisch, M. Gonzalez-Silveira, S. Lenk, J. Rodríguez-Viejo, and S. Reineke, Sci. Adv. 4, eaar8332 (2018).
- <sup>18</sup>S. V. Sreenivasan, Microsyst. Nanoeng. 3, 17075 (2017).
- <sup>19</sup>S. Rhee, J. H. Chang, D. Hahm, K. Kim, B. G. Jeong, H. J. Lee, J. Lim, K. Char, C. Lee, and W. K. Bae, ACS Appl. Mater. Interfaces 11, 40252 (2019).
- <sup>20</sup>Z. K. Tan, R. S. Moghaddam, M. L. Lai, P. Docampo, R. Higler, F. Deschler, M. Price, A. Sadhanala, L. M. Pazos, D. Credgington, F. Hanusch, T. Bein, H. J. Snaith, and R. H. Friend, Nat. Nanotechnol. 9, 687 (2014).
- <sup>21</sup>L. Hou, X. Zhang, G. F. Cotella, G. Carnicella, M. Herder, B. M. Schmidt, M. Pätzel, S. Hecht, F. Cacialli, and P. Samori, Nat. Nanotechnol. 14, 347 (2019).